Taylor & Francis
Taylor & Francis Group

Journal of the Air & Waste Management Association

ISSN: 1096-2247 (Print) (Online) Journal homepage: http://www.tandfonline.com/loi/uawm20

Factor Analysis of Submicron Particle Size Distributions near a Major United States–Canada Trade Bridge

David Ogulei , Philip K. Hopke , Andrea R. Ferro & Peter A. Jaques

To cite this article: David Ogulei , Philip K. Hopke , Andrea R. Ferro & Peter A. Jaques (2007) Factor Analysis of Submicron Particle Size Distributions near a Major United States–Canada Trade Bridge, Journal of the Air & Waste Management Association, 57:2, 190-203, DOI: 10.1080/10473289.2007.10465316

To link to this article: http://dx.doi.org/10.1080/10473289.2007.10465316

Published online: 29 Feb 2012.

Submit your article to this journal

Article views: 137

View related articles

Citing articles: 16 View citing articles

Full Terms & Conditions of access and use can be found at
http://www.tandfonline.com/action/journalInformation?journalCode=uawm20

Download by: [University of North Texas] **Date:** 18 January 2017, At: 16:57

TECHNICAL PAPER

ISSN 1047-3289 *J. Air & Waste Manage. Assoc.* **57**:190–203
Copyright 2007 Air & Waste Management Association

Factor Analysis of Submicron Particle Size Distributions near a Major United States–Canada Trade Bridge

David Ogulei and Philip K. Hopke
Department of Chemical and Biomolecular Engineering, Clarkson University, Potsdam, NY

Andrea R. Ferro
Department of Civil and Environmental Engineering, Clarkson University, Potsdam, NY

Peter A. Jaques
Department of Biology, Clarkson University, Potsdam, NY

ABSTRACT

A factor analytic model has been applied to resolve and apportion particles based on submicron particle size distributions downwind of a United States–Canada bridge in Buffalo, NY. The sites chosen for this study were located at gradually increasing distances downwind of the bridge complex. Seven independent factors were resolved, including four factors that were common to all of the five sites considered. The common factors were generally characterized by the existence of two or more number and surface area modes. The seven factors resolved were identified as follows: fresh tail-pipe diesel exhaust, local/street diesel traffic, aged/evolved diesel particles, spark-ignition gasoline emissions, background urban emissions, heavy-duty diesel agglomerates, and secondary/transported material. Submicron (<0.5 μm) and ultrafine (<0.1 μm) particle emissions downwind of the bridge were dominated by commercial diesel truck emissions. Thus, this study obtained size distinction between fresh versus aged vehicle exhaust and spark-ignition versus diesel emissions based on the measured high time-resolution particle number concentrations. Because this study mainly used particles <300 nm in diameter, some sources that would usually exhibit number modes >100 nm were not resolved. Also, the resolved profiles suggested that the major number mode for fresh tailpipe diesel exhaust might exist below the detection limit of the spectrometer used. The average particle number contributions from the resolved factors were highest closest to the bridge.

IMPLICATIONS

The use of highly time-resolved size distribution measurements has enabled the resolution of different size categories of vehicle emissions. Although the spectrometer used was capable of measuring particles >6 nm in diameter, the results suggest that the major number mode for fresh tailpipe diesel exhaust might exist below the instrument's detection limit. The present study also suggests that there may be at least two nuclei modes associated with diesel exhaust.

INTRODUCTION

In recent years, submicron particles, especially ultrafine particles ([UFPs] <0.1 μm in diameter), have attracted much attention because of an increasing number of studies suggesting an important role played by UFPs in causing adverse health effects in sensitive populations.[1–7] These health effects have been suggested to result from the ability of UFPs to translocate from the respiratory system into the cardiovascular and central nervous systems as demonstrated in animal models.[1,7] Toxic effects have been observed from combustion particles,[8–11] especially from motor vehicle exhaust (for urban areas). The toxicity of motor vehicle exhaust is partly because it consists of organic compounds and oxidant gases that are thought to contribute to the inflammatory and other effects of inhaled particles.[12,13]

Generally, traffic is the primary source of UFPs in urban areas and near busy roadways.[14–22] Cohort studies have typically reported a much higher risk for cardiovascular events for people who live within 150 m of a major highway.[23] A recent study by Peters et al.[24] found a consistent association between the time spent in cars, on public transportation, or on motorcycles and an increase in the risk of myocardial infarction.

In addition to cardiovascular risks, Lwebuga-Mukasa et al.[25] report that the number of households with at least one asthmatic child present in the home is about two times higher downwind than upwind of a major trade bridge in Buffalo, NY. The increased asthma prevalence rate downwind of the international bridge in Buffalo (Peace Bridge Complex [PBC]) has been hypothesized to be related to the increased heavy diesel truck traffic emissions that are dispersed into the community by the prevailing southwesterly winds. Oyana et al.[26] found a clustering of asthma cases in close proximity to the PBC and the associated highways, as well as a dose-response relationship, suggesting a decreased risk of asthma prevalence farther away from this source of exposure.

The Peace Bridge connects Fort Erie, Ontario, Canada, to Buffalo with an estimated annual vehicle count of 6.5 million passenger cars and 1.4 million commercial vehicles, making it one of the busiest United States-Canada

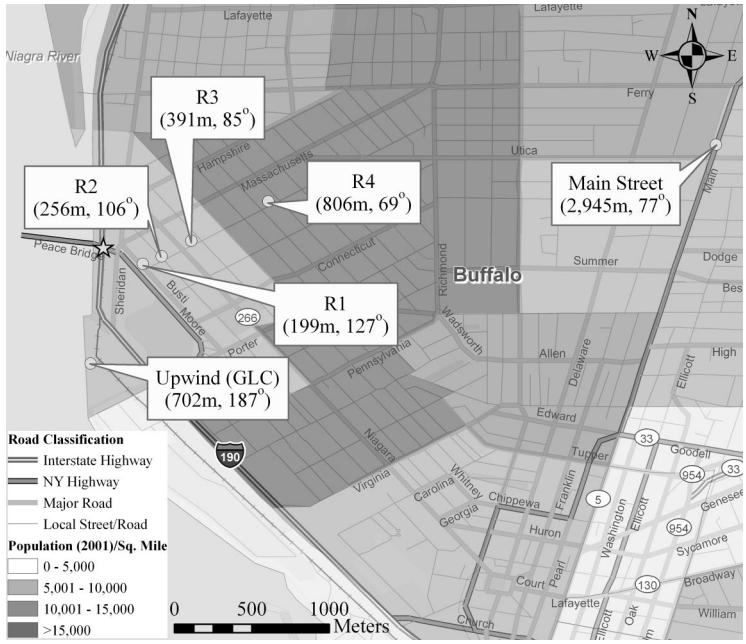

Figure 1. Map showing the location of the sampling sites used in this study. The reported distances are measured relative to an arbitrary center point of the Peace Bridge (marked with a star on the map). The wind direction was generally southwesterly over the sampling period.

border crossings in the northeast. Because UFPs are dominated by freshly generated (typically nuclei mode) particles, freshness and proximity to the source may, thus, be key requirements for inducing adverse health effects of UFPs.[27]

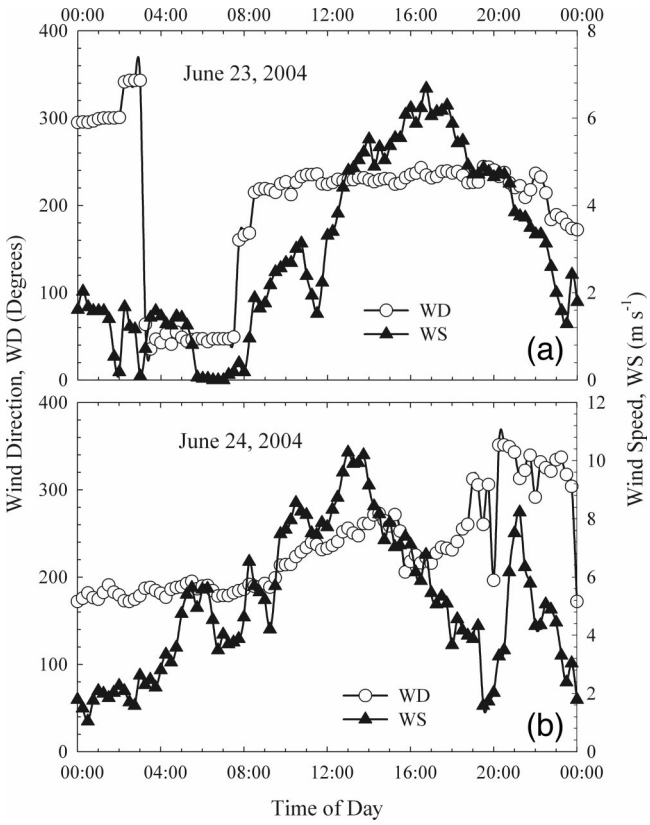

Figure 2. Observed wind profiles on June 23 (a) and 24 (b), 2004, as measured at the GLC (upwind site). The measurements are 15-min averages.

An appropriate metric for characterizing submicron or UFPs is their size distribution, because each size class will generally have different penetrability and deposition patterns in the respiratory tract.[28–31] On-road submicron particle number size distributions typically contain an accumulation mode with an estimated mean diameter of 100 nm, consisting of carbonaceous agglomerates.[21,22] Diesel and spark ignition vehicles also contribute to the occurrence of a nuclei mode that is between 5 and 50 nm in diameter.[21,32–35]

Once particles are emitted from a source, their size, number, and chemical composition change by several mechanisms until they are ultimately removed by atmospheric processes.[15–17,35,36] However, the particle size distributions would be expected to remain approximately stationary at any given location relative to the emission source. Moreover, over a short measurement period, the effect of changes in photochemical activity, ambient temperature, or humidity that have the potential of influencing the particle size distribution may be treated as relatively constant. Thus, the observed size distributions at the receptor site can be treated as a linear sum of size distributions from all of the contributing emission sources, thus permitting the application of factor analysis methods for source resolution and apportionment.

In respect to the above, the objective of the present study was to use a factor analytic model, positive matrix factorization (PMF)2,[37] to resolve the different size distributions associated with submicron particle emissions near the PBC and to apportion these distributions to their sources. Highly time-resolved (1 sec) number concentrations measured at multiple sites downwind of the bridge were used as inputs to the model. With prevailing winds from the southwest, UFP concentrations downwind of the PBC were dominated by congested bridge traffic, including emissions from diesel trucks waiting to clear customs. This study aims to distinguish between fresh versus aged

Table 1. Summary statistics for all of the sites (cm^{-3}), at 1-sec resolution.

Site Name	R1	R2	R3	R4	Main Street	Upwind
N	3737	1764	1189	423	4680	30553
Arithmetic mean	8.37E+04	4.54E+04	3.82E+04	1.93E+04	2.46E+04	1.39E+04
Arithmetic standard deviation	3.40E+04	1.35E+04	1.21E+04	5.06E+03	2.87E+04	1.21E+04
Geometric mean	7.83E+04	4.36E+04	3.68E+04	1.86E+04	1.86E+04	1.13E+04
Geometric standard deviation	1.43	1.32	1.29	1.29	1.93	1.82
Minimum	2.70E+04	2.43E+04	1.99E+04	1.16E+04	4.05E+03	2.26E+03
Median	7.63E+04	4.42E+04	3.63E+04	1.81E+04	1.77E+04	1.03E+04
Maximum	3.93E+05	1.37E+05	1.28E+05	4.12E+04	3.71E+05	2.35E+05

Notes: R1 to R4 measurements were made on June 24, 2004, whereas Main St. values were obtained on June 23. Upwind measurements were made on June 23 and 24, 2004.

vehicle exhaust and spark-ignition versus diesel emissions based on their size distributions with very short-duration size distribution measurements. Limited numbers of studies have measured the size distributions of diesel emissions using on-road and laboratory measurements,[16,20,32–34,38–40] but these studies have typically relied on lower time-resolved measurements with scan times of >1 min. Yao et al.[36,41] used a mobile platform equipped with several instruments, including an engine exhaust particle spectrometer (EEPS), to measure submicron particle (5.6–560 nm) concentrations in streets and tunnels at measurement times of 1 and 3.2 sec. Thus, results from real-time measurements and apportionment of vehicle exhaust size distributions in transient scenarios are generally limited or unavailable.

Laboratory particle measurements on emissions from new European diesel engines have reported significant size differences between primary particles emitted from new and older engines.[42] Thus, the present methodology may also provide a basis for application in real-time size distinction of particle emissions from new and older engines.

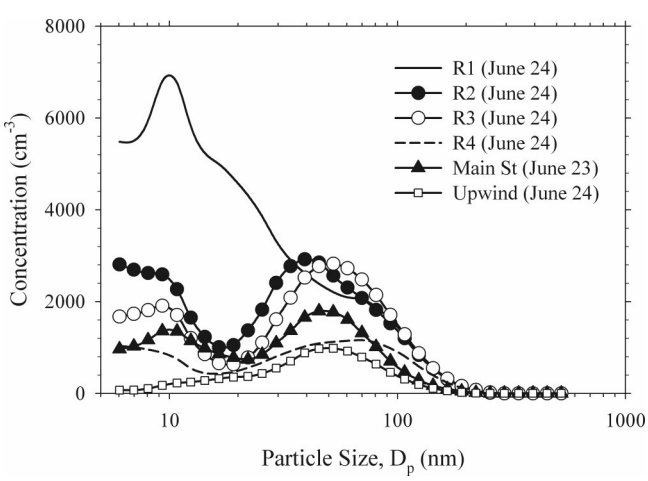

Figure 3. Average number concentrations measured at the six sampling sites. Sample resolution was 1 sec for all of the sites. On June 24, winds consistently blew from the southwest. For completeness, the entire particle size range measured (6–500 nm) is shown.

EXPERIMENTAL WORK

Data and Sites Description

The data used in this study were obtained on June 23 and 24, 2004, from multiple sampling sites in Buffalo. The sites were selected so as to enable size classification of the dispersing plumes from the Peace Bridge, while at the same time enabling the study of background concentrations at an upwind site (Great Lakes Center [GLC]; Figure 1). During the study period, there were idling trucks at the bridge's toll and customs plaza providing the potential for elevated concentrations downwind of the bridge. Downwind sites were located within a distance expected to be affected by UFPs emitted directly from the PBC (i.e., sites R1, R2, R3, and R4), as well as local urban street traffic emissions (Main Street site; Figure 1).

Near real-time number concentrations of particles in the size range 6–500 nm were measured using an EEPS (TSI Model 3090[43]). The EEPS uses an electrical mobility technique similar to that of the scanning mobility particle sizer ([SMPS] TSI Inc.). In contrast to the SMPS, the EEPS has a higher time resolution (down to 0.1 sec per scan; 32 channels) by using a series of electrometers that provide simultaneous measurement of multiple particle sizes. Thus, it is an instrument of choice for studying transient engine emissions in near real time. Developed for engine emissions measurement, the EEPS has recently been used to evaluate emission control devices during on-road tests.[44] The EEPS was incorporated into Clarkson University's Mobile Air Pollution Laboratory. Samples were ducted to the instrument through a manifold connected to an inlet located 2 m above the roof of the mobile van with a sample flow rate of 10 L/min providing minimal diffusion losses of the smaller particles.

Raw data were acquired at 0.1-sec resolution and integrated to 1, 2, and 5 sec for subsequent analyses. Samples for sites R1 to R4 were collected on June 24, 2004, whereas the Main Street samples were collected on June 23, 2004. Upwind measurements were made throughout June 23 and 24, 2004 (30,553 valid 1-sec samples). R1 measurements were made from 10:14:20 a.m. to 1:39:51 p.m. (3737 valid 1-sec samples); R2 from 1:50:55 p.m. to 2:20:55 p.m. (1764 valid 1-sec samples); R3 from 2:43:10 p.m. to 3:02:59 p.m. (1189 valid 1-sec samples); R4 from 3:30:25 p.m. to 3:37:28 p.m. (423 valid 1-sec samples); and Main Street from 3:29:00 p.m. to 4:57:00 p.m. (4680 valid 1-sec samples). For modeling purposes, R1 and Main

Table 2. A sample of events recorded during the sampling campaign reported in this study.

Event Identification	Event Description	Maximum Total Concentration (cm^{-3})	Start Time (p.m.)
June 24, 2004			
S1	Idling Ford truck next to MAPL (R1 only)	139,983.10	1:28:30
S2	Large truck passed (R3 only)	128,210.67	2:55:03
June 23, 2004			
S3	Fixed site by gas station (Main Street); 18 cars per min; Bus station SE of site	16,482.83	3:29:10
S4	Fixed site by gas station (Main Street); 18 cars per min; Bus station SE of site	211,596.47	3:29:51
S5	Heavy diesel truck passed	23,743.78	4:01:24
S6	Heavy diesel truck passed	18,311.97	4:01:38
S7	Heavy diesel truck passed	21,437.93	4:10:53
S8	Large bus passed	37,204.80	4:11:21
S9	Large bus passed	85,947.83	4:11:35
S10	NFTA bus passing	70,990.92	4:23:02
S11	Metro bus passing	54,749.80	4:25:15
S12	Bus passing	49,522.56	4:28:34
S13	Electric utilities truck passing	17,476.29	4:30:37
S14	Electric utilities truck passing	19,002.99	4:30:51
S15	School bus passing	15,213.05	4:31:31
S16	NFTA bus idling at SE bus stop	20,221.27	4:32:40
S17	NFTA bus idling at SE bus stop	15,988.75	4:32:55
S18	NFTA bus idling at SE bus stop	18,500.50	4:33:20
S19	LaidLaw school bus passing	32,395.61	4:34:41
S20	Tow truck passing	202,873.12	4:35:52
S21	Metro bus passing	17,236.97	4:36:57
S22	Two buses passing	83,799.67	4:38:33
S23	Two buses passing	251,025.02	4:39:23
S24	Two NFTA buses idling at SE corner stop	34,875.18	4:42:52
S25	Metro bus passing, stopping at nearby light to turn left	44,780.85	4:47:57
S26	Metro bus makes the left turn	107,967.29	4:48:42
S27	Metro bus passing	24,155.83	4:51:36
S28	Metro bus passing	40,735.14	4:52:45
S29	Metro bus at bus stop SE of MAPL	70,684.56	4:55:06
S30	Metro bus left the station	119,807.38	4:56:00

Notes: With the exception of S1 and S2, all of the events were recorded at the Main Street site.

Street data were integrated to 5-sec resolution, whereas R2 data were integrated to 2 sec, leading to 747, 882, and 936 samples for R1, R2, and Main Street, respectively. The measured wind speed and directions are presented in Figure 2. The wind consistently blew from the southwest and west.

The total number concentrations measured in this study are summarized in Table 1. For completeness, the entire particle size range measured (6–500 nm) is shown, although the concentration of particles >300 nm was generally below the instrument's detection limit (>80% of samples). Data from the upwind site were only used to provide an estimate of the background concentrations/size distributions, but were not analyzed. It can be seen that the total concentrations gradually decreased away from the Peace Bridge, with an approximately equivalent spread in the distributions (i.e., nearly identical geometric standard deviations) among the four sites (R1 to R4). The upwind site recorded the lowest average concentrations (13,919 ± 12,108 cm^{-3}), whereas the highest values were observed at R1 (83,737 ± 33,966 cm^{-3}). Overall, these values are higher than the values reported for the cities of Rochester, NY,[45–47] and Gothenburg, Sweden,[22] but are comparable to the average values reported in Atlanta, GA,[48] Pittsburgh, PA,[49] Baltimore, MD,[50] and near Los Angeles, CA, freeways.[15–17] The observed difference between the average values measured in this study and those obtained in Rochester and Gothenburg is probably because of the larger size range considered in this study (the size range for the Rochester study was 11–470 nm, whereas that for Gothenburg was 10–368 nm). The measured average size distributions are shown in Figure 3.

Table 2 lists some of the events/activities observed during the sampling campaign. These events often led to significant increases in the measured particle number concentrations. To effect comparisons with profiles predicted from this study, the size distributions of some of these events/activities are presented in Figure 4.

Model Description

Assuming the measured size distributions are stationary (or quasistationary), the bilinear receptor model PMF2 finds the least-squares solution of the component equation:

$$N_{ij} = \sum_{k=1}^{p} g_{ik} f_{kj} + e_{ij} \quad (1)$$

in which N_{ij} is the measured particle number concentration of the jth size bin in the ith sample; f_{kj} is the

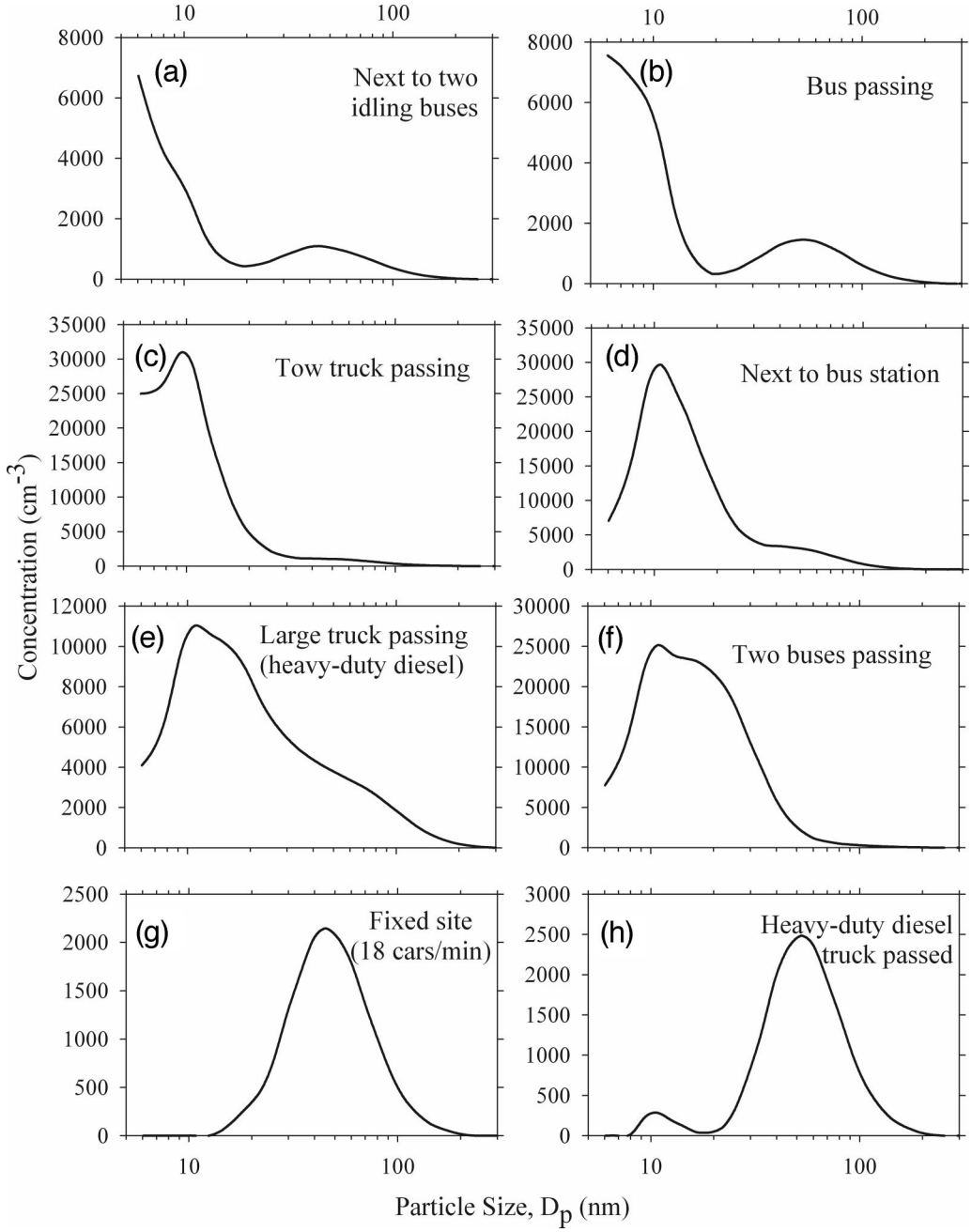

Figure 4. Characteristics of some of the events listed in Table 2. Most of the events were observed at the Main Street site: (a) next to two idling buses; (b) bus passing; (c) tow truck passing; (d) next to bus station; (e) large truck passing (heavy-duty diesel); (f) two buses passing; (g) fixed site (18 cars/min); (h) heavy-duty diesel truck passed.

concentration of the jth size bin in material emitted by the kth source; g_{ik} is the contribution of the kth source to the ith sample; and e_{ij} is the residual. The model can then be used to estimate the optimum number, p, of independent sources (or factors) that adequately explain the observations at each sampling site. In this study, the five sites (R1, R2, R3, R4, and Main Street) were analyzed independently.

Because of the high fraction of values below the detection limit, or zero values, for size bins ≥300 nm in the original data (>80%), only concentration values for sizes <300 nm were used. Generally, the percentage of zero values in the data increased as one moved away from the bridge area.

Equation 1 requires the availability of measurement uncertainties for each (i, j) data point. However, because no measurement uncertainties were available, the required uncertainties were estimated from the following equation[47,51]:

$$\sigma_{ij} = \begin{cases} 0.01(N_{ij} + \bar{N}j) & \text{if } N_{ij} > 0 \\ 2\bar{N}j & \text{if } N_{ij} = 0 \end{cases} \quad (2)$$

where σ_{ij} is the calculated (estimated) measurement error for size bin j and sample i; N_{ij} is the observed number concentration; and $\bar{N}_j$ is the arithmetic mean of the reported values for N_j.

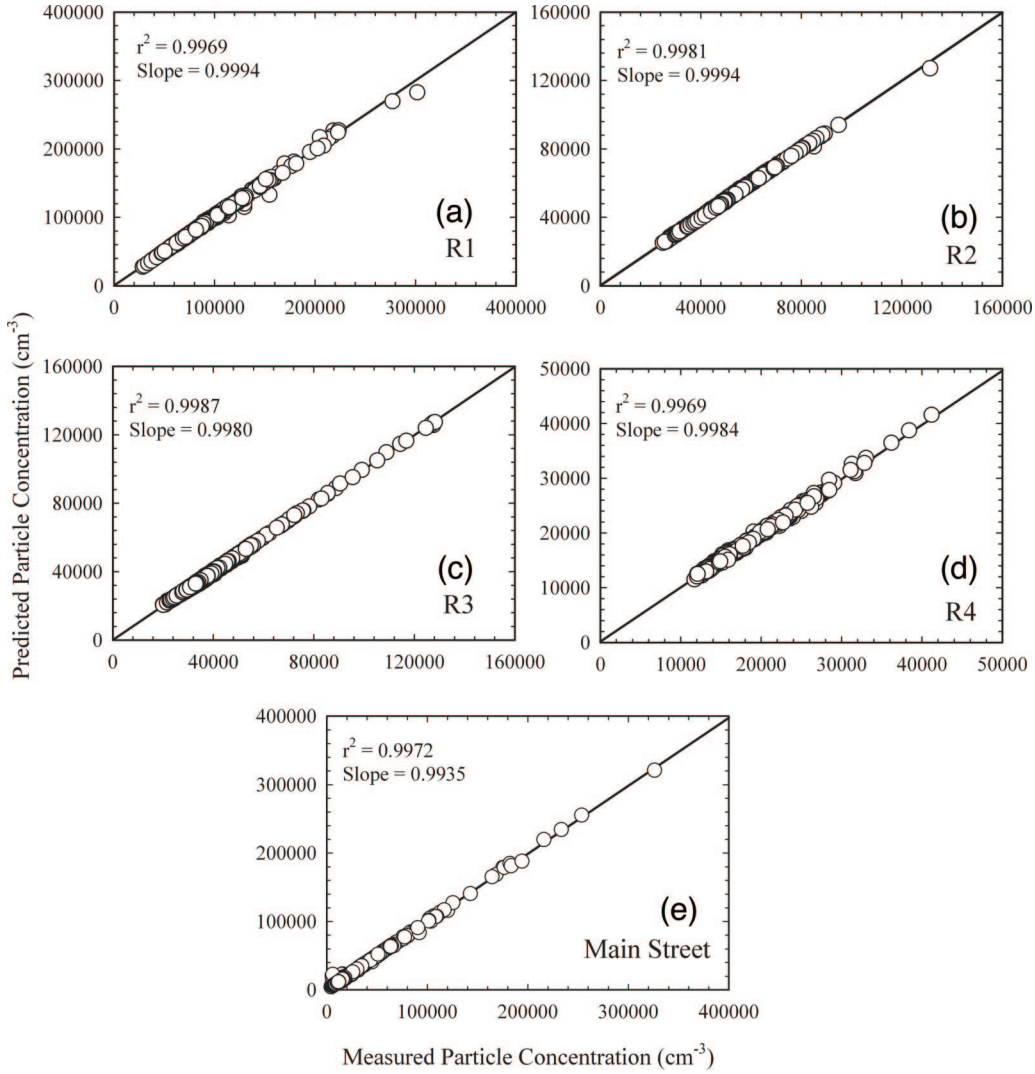

Figure 5. A plot of the PMF2-predicted number concentrations vs. the measured concentrations for all of the sites. The five sites were analyzed independently. Only particle sizes <300 nm were used in the model. (a) R1; (b) R2; (c) R3; (d) R4; (e) Main Street.

The PMF2 algorithm includes several error models that can be used to compute heuristic error estimates (s_{ij}) based on the data points and their original measurement error estimates. The error model equation used in this study was:

$$s_{ij} = \sigma_{ij} + C_3\ (N_{ij}) \tag{3}$$

where σ_{ij} is the estimated measurement error (eq 2), and C_3 is a constant, chosen such that the scaled residuals (e_{ij}/s_{ij}) are approximately randomly distributed between -2 and $+2$. The appropriate value of C_3 for each dataset was determined by varying C_3 from 0.001 to 0.3 and computing the corresponding model estimates.

The results (source profiles and source contributions) were rescaled to the measured number concentrations using a scaling constant, s_k, obtained by regressing the measured total number concentrations against the estimated source contributions, g_{ik}, according to eq 4:

$$N_{ij} = \sum_{k=1}^{p} (s_k) g_{ik} \tag{4}$$

Optimum Number of Factors. The optimum number of factors, p, is determined based on the quality of the fit and the interpretability of the model results. The experimental residual sum of squares, Q, for k factors should approach its theoretical value, defined as the total number of data points minus the number of degrees of freedom, that is, $(n \times m) - [(n \times k) + (m \times k)]$. For each value of C_3 (eq 3), p was varied from 4 to 9 or higher until the obtained Q value was very close to the theoretical value. Final C_3 values were 0.017 (R1), 0.008 (R2), 0.03 (R3), 0.03 (R4), and 0.08 (Main Street) corresponding with p of 6, 6, 5, 5, and 6, respectively.

The method of G-space plotting was used to study the rotational ambiguity of the emerging solutions.[52] Final values of the rotational parameter, FPEAK, were 0 for all of the datasets, corresponding with calculated Q values of

Table 3. Pearson's product moment correlation coefficients between the predicted profiles and all of the observed events listed in Table 2.

	Factor 1					Factor 2				
Event ID	R1	R2	R3	R4	Main Street	R1	R2	R3	R4	Main Street
S1	0.01	−0.12	0.01	−0.08	−0.04	0.56	0.33	0.36	0.23	0.58
S2	0.30	0.07	0.27	0.09	0.23	0.84[a]	0.65	0.68	0.58	0.84[a]
S3	−0.40	−0.30	−0.21	−0.27	−0.37	−0.38	−0.03	−0.26	−0.17	−0.42
S4	0.47	0.16	0.39	0.16	0.39	0.97[a]	0.80[a]	0.85[a]	0.78[a]	0.97[a]
S5	−0.43	−0.36	−0.27	−0.33	−0.42	−0.25	0.03	−0.11	−0.09	−0.31
S6	−0.36	−0.29	−0.19	−0.28	−0.34	−0.28	0.08	−0.07	−0.01	−0.35
S7	−0.01	−0.11	0.12	−0.10	−0.03	0.27	0.56	0.42	0.46	0.18
S8	0.83[a]	0.72[a]	0.89[a]	0.72[a]	0.82[a]	0.44	0.64	0.51	0.60	0.36
S9	0.63	0.38	0.58	0.38	0.57	0.88[a]	0.75[a]	0.76[a]	0.71[a]	0.86[a]
S10	0.55	0.27	0.50	0.27	0.48	0.93[a]	0.80[a]	0.81[a]	0.76[a]	0.92[a]
S11	0.51	0.49	0.63	0.49	0.51	0.23	0.47	0.35	0.41	0.13
S12	0.97[a]	0.85[a]	0.97[a]	0.83[a]	0.96[a]	0.48	0.58	0.51	0.59	0.42
S13	−0.29	−0.35	−0.12	−0.32	−0.30	0.14	0.35	0.15	0.18	0.11
S14	0.51	0.50	0.64	0.51	0.51	0.18	0.45	0.28	0.36	0.09
S15	0.03	−0.20	0.12	−0.20	−0.02	0.60	0.79[a]	0.66	0.69	0.55
S16	0.89[a]	0.83[a]	0.95[a]	0.83[a]	0.89[a]	0.30	0.50	0.36	0.47	0.22
S17	0.19	−0.03	0.28	−0.02	0.14	0.64	0.79	0.65	0.67	0.59
S18	0.66	0.42	0.68	0.42	0.61	0.80[a]	0.86[a]	0.80[a]	0.81[a]	0.75[a]
S19	−0.15	−0.18	−0.07	−0.13	−0.16	0.23	0.12	0.04	−0.03	0.26
S20	0.87[a]	0.63[a]	0.80[a]	0.62	0.81[a]	0.78[a]	0.73[a]	0.72[a]	0.74[a]	0.75[a]
S21	0.94[a]	0.92[a]	0.98[a]	0.91[a]	0.95[a]	0.22	0.38	0.27	0.38	0.15
S22	0.99[a]	0.92[a]	0.98[a]	0.91[a]	0.98[a]	0.36	0.44	0.38	0.46	0.30
S23	0.30	0.08	0.25	0.10	0.23	0.78[a]	0.53[a]	0.57	0.46	0.80[a]
S24	0.98[a]	0.93[a]	0.99[a]	0.93[a]	0.97[a]	0.33	0.41	0.33	0.40	0.28
S25	0.64	0.44	0.64	0.45	0.59	0.76	0.68[a]	0.63	0.61	0.74[a]
S26	1.00[a]	0.91[a]	0.97[a]	0.89[a]	0.98[a]	0.42	0.46	0.41	0.48	0.37
S27	−0.06	0.02	0.10	0.03	−0.04	−0.20	0.14	0.01	0.08	−0.29
S28	0.83[a]	0.60[a]	0.79[a]	0.59	0.77[a]	0.80[a]	0.75[a]	0.73[a]	0.73[a]	0.76[a]
S29	1.00[a]	0.94[a]	0.99[a]	0.93[a]	0.99[a]	0.34	0.40	0.34	0.42	0.29
S30	0.34	0.06	0.27	0.06	0.26	0.93[a]	0.70[a]	0.77[a]	0.67	0.94[a]

Notes: [a]Coefficients >0.70.

15,178; 18,343; 27,258; 10,707; and 18,814 and theoretical values of 15,525; 18,360; 26,023; 9171; and 19,494 for R1, R2, R3, R4, and Main Street sites, respectively. A plot of the predicted particle number concentrations versus the measured concentrations is provided in Figure 5.

RESULTS AND DISCUSSION

Seven factors were resolved in this analysis, of which four factors were common to all five of the sites. The factors were generally characterized by the existence of two or more number and surface area modes. The surface area and volume distributions were estimated by assuming spherical particles. Because particles >300 nm in diameter were generally below the detection limits, those sources that would usually exhibit number modes >300 nm were not well resolved in the analysis. Tables 3–5 show the Pearson's product moment correlation coefficients between all of the resolved factors and the size distributions of the observed events/activities. This approach provides a practical way of directly comparing the predicted size distributions with the observed distributions. The average contributions resolved in this analysis are shown in Table 6.

Factor 1

This factor displays two number modes, with the smaller mode falling below the 5.6 nm detection limit of the EEPS (Figure 6). The larger mode falls between 30 and 50 nm at all sites. This factor was found to be highly correlated with emissions from passing and idling buses and trucks (Table 3 and Figure 4, a–c) and is thought to represent fresh tailpipe diesel exhaust particles. Average contributions were highest at R1, probably because of high levels of emissions from the idling diesel trucks at the Peace Bridge (Table 6). The lowest average contribution was observed at R4. Concentrations decreased approximately exponentially from R1 to R4 in a similar fashion as reported by Zhu et al.[16] R1 concentrations were ~2.4 times higher than the closest site, R2, and ~11.4 times higher than R4 (Figure 7). Because previous studies on diesel emissions have typically relied on particles >10 nm in diameter, only the larger mode has generally been reported. Kittelson[32] and Kittelson et al.[33] indicate that a single nuclei mode from diesel exhaust particles exists between the broad range of 5–50 nm. The present study suggests that there may be at least two modes in this size range.

Factor 2

The number profiles for factor 2 is bimodal over the size range considered in this study. These size distribution profiles are similar to those reported by Kittelson et al.[20,33] and Kittelson[32] for diesel particles. The nuclei mode is ~10 nm, whereas the accumulation mode is at

Table 4. Pearson's product moment correlations continued.

Event Identification	Factor 3					Factor 4				
	R1	R2	R3	R4	Main Street	R1	R2	R3	R4	Main Street
S1	0.95[a]	0.87[a]	0.93[a]	0.74[a]	0.74[a]	0.39	0.33	−0.20	−0.36	−0.24
S2	0.86[a]	0.60	0.73[a]	0.41	0.41	0.09	0.06	−0.31	−0.46	−0.29
S3	−0.22	0.02	0.12	0.42	0.33	0.74[a]	0.84[a]	0.92[a]	0.81[a]	0.90[a]
S4	0.69	0.31	0.45	0.03	0.05	−0.24	−0.27	−0.49	−0.58	−0.43
S5	−0.16	0.03	0.10	0.35	0.24	0.59	0.71[a]	0.94[a]	0.84[a]	0.94[a]
S6	−0.37	−0.21	−0.12	0.14	0.03	0.48	0.61	0.98[a]	0.90[a]	0.99[a]
S7	−0.04	−0.11	0.07	0.10	0.00	0.33	0.45	0.74[a]	0.61	0.78[a]
S8	−0.04	−0.29	−0.11	−0.23	−0.23	−0.07	−0.03	0.06	−0.04	0.13
S9	0.66	0.30	0.45	0.08	0.12	−0.15	−0.18	−0.45	−0.57	−0.40
S10	0.67	0.30	0.46	0.07	0.10	−0.15	−0.18	−0.45	−0.56	−0.40
S11	−0.04	−0.11	0.02	0.06	0.02	0.26	0.32	0.47	0.36	0.49
S12	−0.02	−0.32	−0.18	−0.37	−0.32	−0.29	−0.29	−0.28	−0.33	−0.21
S13	0.31	0.40	0.56	0.64	0.57	0.76[a]	0.82[a]	0.64	0.46	0.62
S14	−0.07	−0.13	0.03	0.07	0.04	0.30	0.38	0.48	0.34	0.51
S15	0.36	0.19	0.40	0.27	0.21	0.35	0.41	0.41	0.26	0.43
S16	−0.12	−0.32	−0.17	−0.24	−0.21	−0.06	−0.03	0.01	−0.07	0.07
S17	0.45	0.27	0.48	0.33	0.28	0.36	0.41	0.29	0.11	0.32
S18	0.38	0.03	0.23	−0.05	−0.05	−0.08	−0.06	−0.10	−0.23	−0.03
S19	0.81[a]	0.89[a]	0.96[a]	0.93[a]	0.93[a]	0.72[a]	0.66	0.02	−0.17	−0.04
S20	0.32	−0.08	0.06	−0.29	−0.23	−0.39	−0.41	−0.52	−0.58	−0.45
S21	−0.18	−0.38	−0.26	−0.32	−0.28	−0.16	−0.14	−0.10	−0.15	−0.04
S22	−0.09	−0.35	−0.25	−0.40	−0.35	−0.33	−0.33	−0.29	−0.31	−0.22
S23	0.92[a]	0.68	0.78[a]	0.45	0.49	0.09	0.02	−0.50	−0.64	−0.49
S24	−0.04	−0.27	−0.16	−0.30	−0.24	−0.22	−0.22	−0.26	−0.32	−0.20
S25	0.67	0.38	0.54	0.24	0.29	0.06	0.02	−0.38	−0.53	−0.35
S26	−0.01	−0.30	−0.19	−0.39	−0.32	−0.35	−0.36	−0.41	−0.44	−0.34
S27	−0.31	−0.18	−0.10	0.14	0.05	0.47	0.57	0.92[a]	0.84[a]	0.90[a]
S28	0.41	0.04	0.20	−0.13	−0.09	−0.25	−0.26	−0.43	−0.53	−0.36
S29	−0.06	−0.31	−0.21	−0.37	−0.30	−0.31	−0.31	−0.34	−0.38	−0.28
S30	0.82[a]	0.49	0.61	0.21	0.23	−0.13	−0.16	−0.47	−0.58	−0.43

Notes: [a]Coefficients >0.70.

~50–70 nm (Figure 6). This factor is believed to represent local/moving diesel traffic emissions. The observed distributions are comparable with those given in Figure 4, d–f.

Figure 8 shows more frequent spikes at R1 because of the expected influence of the Peace Bridge, whereas the spikes seen at R3 and Main Street occur at times when the events listed in Table 2 were observed. For instance, the sharp spike at R3 occurs at 2:55:03 p.m. corresponding with event S2 (Table 2). At the time of measurements at R1, R2, R3, and R4, the Peace Bridge was continuously congested with idling trucks, and relatively strong winds consistently blew from the southwest (Figure 2). The number concentrations can be seen to significantly decrease away from the Peace Bridge (a factor of ~1.3 from R1 to R2, and 2.8 from R1 to R3; Figure 7). The average contributions at R3, R4, and Main Street were approximately equal at ~5200 particles cm^{-3}.

Factor 3

The size distribution for this factor is bimodal with number modes at ~15–30 nm and 100–130 nm. Although the shapes of the number distributions for this factor are comparable to factor 2 (i.e., bimodal with a sharp nuclei peak), the correlations between this factor and most of the source events are generally poor, whereas factor 2 was highly correlated (Tables 3 and 4). Also, because the size modes are observed at bigger particle sizes than seen in factors 1 and 2, it is evident that this factor represents a different category of diesel particles. This factor may, thus, represent aged diesel particles that have evolved to slightly larger sizes through coagulation and condensation on pre-existing particles. The size distribution is comparable to that reported by Jamriska et al.[53] from their studies in Brisbane, Australia. The average contribution at R1 (24,000 particles cm^{-3}) is ~5.1 times higher than that at R2 and ~6.8 times higher than that at R3, whereas the average contributions at R3, R4, and Main Street are approximately equal at ~3500 particles cm^{-3}.

Factor 4

This factor probably represents spark-ignition gasoline emissions from highway/on-road traffic. Its size distribution is similar to that obtained from measurements made near an intersection of major traffic routes in Rochester.[47] With the exception of the Main Street site, of which the location was least likely affected by dispersed emissions from the Peace Bridge and, thus, potentially more influenced by local urban traffic emissions, the size mode increases with distance along the approximate dispersion center line of Peace Bridge emissions (number modes at

Table 5. Pearson's product moment correlations continued.

Event Identification	Factor 5			Factor 6		Factor 7		
	R2	R3	Main Street	R1	R4	R1	R2	Main Street
S1	−0.21	−0.21	−0.13	−0.34	−0.32	−0.59	−0.31	−0.47
S2	−0.34	−0.32	−0.22	−0.37	−0.42	−0.61	−0.48	−0.52
S3	0.92[a]	0.93[a]	0.97[a]	0.62	0.78[a]	−0.05	0.26	0.10
S4	−0.53	−0.49	−0.40	−0.45	−0.56	−0.51	−0.56	−0.50
S5	0.91[a]	0.93[a]	0.97[a]	0.74[a]	0.82[a]	0.01	0.29	0.15
S6	0.95[a]	0.97[a]	0.99[a]	0.80[a]	0.88[a]	0.12	0.31	0.25
S7	0.67	0.72[a]	0.80[a]	0.58	0.59	−0.17	−0.03	−0.03
S8	−0.01	0.05	0.15	0.02	−0.05	−0.40	−0.44	−0.31
S9	−0.50	−0.46	−0.35	−0.44	−0.54	−0.60	−0.58	−0.55
S10	−0.49	−0.45	−0.35	−0.46	−0.54	−0.58	−0.59	−0.54
S11	0.42	0.46	0.52	0.38	0.36	−0.26	−0.24	−0.07
S12	−0.34	−0.29	−0.21	−0.24	−0.35	−0.38	−0.51	−0.34
S13	0.63	0.66	0.73	0.30	0.46	−0.37	−0.03	−0.20
S14	0.42	0.46	0.56	0.33	0.33	−0.35	−0.24	−0.18
S15	0.37	0.42	0.49	0.22	0.27	−0.35	−0.24	−0.21
S16	−0.05	0.00	0.09	−0.03	−0.09	−0.39	−0.42	−0.31
S17	0.24	0.29	0.40	0.08	0.12	−0.50	−0.34	−0.35
S18	−0.17	−0.11	0.00	−0.14	−0.22	−0.51	−0.53	−0.42
S19	0.04	0.03	0.11	−0.26	−0.13	−0.61	−0.16	−0.46
S20	−0.58	−0.53	−0.45	−0.45	−0.58	−0.46	−0.61	−0.46
S21	−0.15	−0.11	−0.03	−0.09	−0.17	−0.34	−0.41	−0.28
S22	−0.34	−0.30	−0.23	−0.21	−0.33	−0.31	−0.47	−0.28
S23	−0.52	−0.50	−0.41	−0.57	−0.60	−0.65	−0.48	−0.59
S24	−0.31	−0.28	−0.19	−0.24	−0.33	−0.40	−0.49	−0.35
S25	−0.42	−0.38	−0.27	−0.47	−0.51	−0.69	−0.57	−0.59
S26	−0.46	−0.42	−0.35	−0.34	−0.46	−0.37	−0.51	−0.36
S27	0.88[a]	0.90[a]	0.92[a]	0.78[a]	0.83[a]	0.06	0.16	0.25
S28	−0.49	−0.44	−0.34	−0.41	−0.52	−0.55	−0.61	−0.51
S29	−0.39	−0.36	−0.28	−0.29	−0.40	−0.36	−0.49	−0.34
S30	−0.51	−0.48	−0.39	−0.46	−0.55	−0.55	−0.52	−0.51

Notes: [a]Coefficients >0.70.

~30, 35, 55, and 70 nm at R1, R2, R3, and R4, respectively; Figure 6). The observed increase in particle size with distance from the bridge is consistent with previous observations near major freeways consisting of a high percentage of spark-ignition vehicles.[15,17,54] The time series for this factor (Figure 8) suggests relatively steady traffic at R3 and R4 over the period considered, as would be expected from spark-ignition traffic. It should be noted that the average contribution at R2 is lower than at R3 potentially because of the influence of the major road (Route 266) that runs southeast/northwest upwind of site R3. Also, the average contribution at R1 is comparable to that at R3 (12,000 vs. 10,200 particles cm^{-3}, respectively), but is much higher than at R4 (2100 particles cm^{-3}) or Main Street (1070 particles cm^{-3}; Table 6). Ristovski et al.[55] reported bimodal size distributions from spark-ignition vehicles with average values of the count median diameter (CMD) ranging from 39.1 to 60.2 nm within the range measured by the SMPS used.

Factor 5

This factor is thought to represent background urban emissions, presumably from traffic-related sources. This factor was not resolved at R1, which suggests a stronger

Table 6. Average source contributions (cm^{-3}) from all of the resolved factors.

Resolved Factor	R1	R2	R3	R4	Main Street
Fresh tailpipe diesel exhaust (factor 1)	21450 (25.5)	8910 (19.6)	8084 (21.2)	1887 (9.8)	3812 (15.4)
Local/street diesel traffic (factor 2)	16195 (19.3)	12094 (26.6)	5789 (15.2)	5227 (27.1)	5250 (21.2)
Aged/processed diesel particles (factor 3)	24287 (28.9)	4718 (10.4)	3549 (9.3)	3526 (18.3)	3844 (15.5)
Spark-ignition gasoline emissions (factor 4)	12053 (14.3)	6475 (14.2)	10207 (26.7)	2106 (10.9)	1075 (4.3)
Urban background emissions (factor 5)		13097 (28.8)	10583 (27.7)		9760 (39.5)
Heavy-duty diesel agglomerates (factor 6)	9173 (10.9)			6530 (33.9)	
Secondary/transported material (factor 7)	845 (1.0)	159 (0.3)			995 (4.0)

Notes: Numbers in parentheses are the percentage contributions at each site (calculated with respect to all the resolved sources at that site).

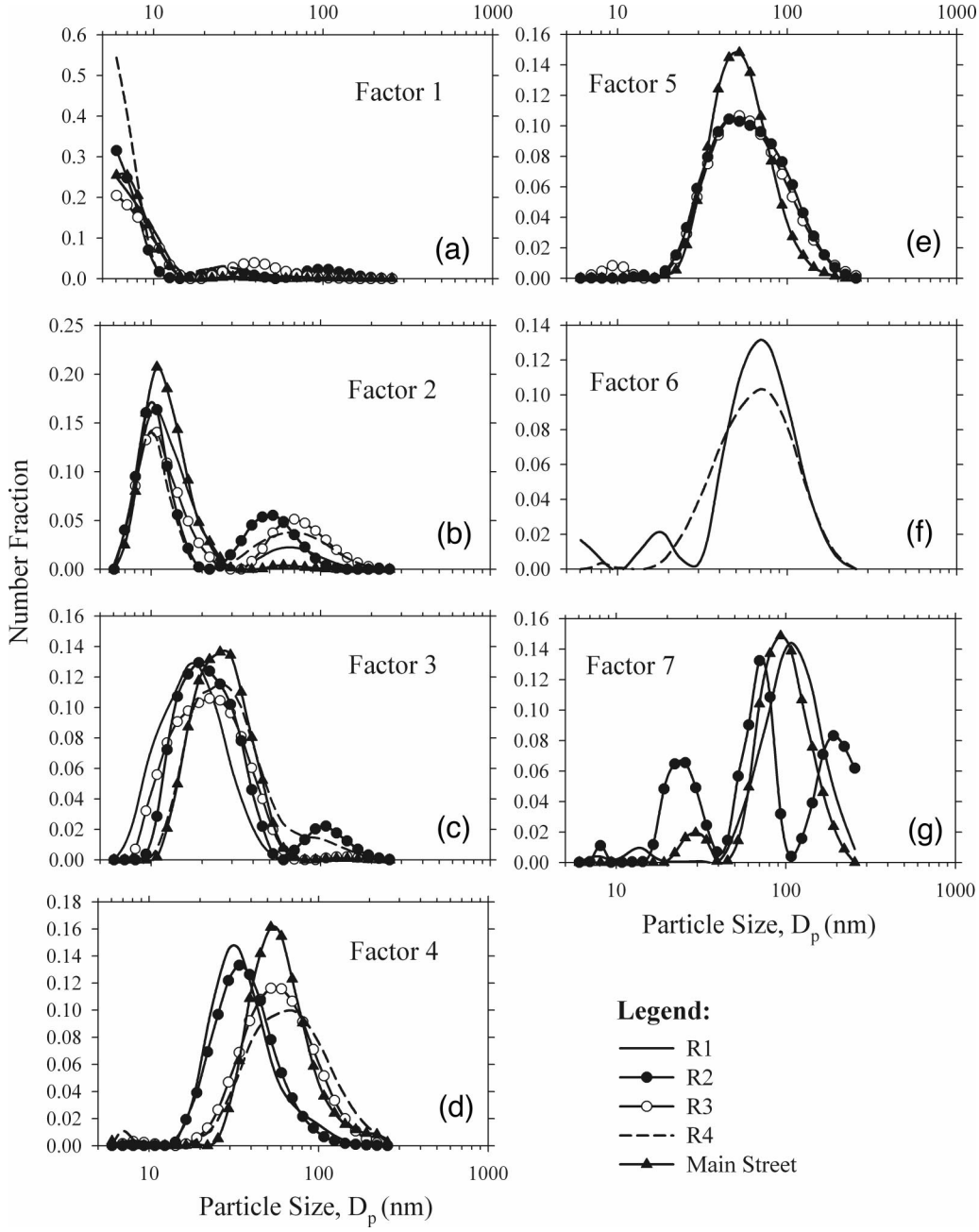

Figure 6. PMF2-resolved number profiles. Four factors were common to all of the five datasets, with R1 generally producing smaller modes for primary Peace Bridge emissions. (a) Factor 1; (b) factor 2; (c) factor 3; (d) factor 4; (e) factor 5; (f) factor 6; (g) factor 7.

influence of non-Peace Bridge emissions, because the sites R2, R3, and Main Street were also characterized by moderate local urban emissions. The major mode is at 50 nm, and the size distribution is comparable to the average distribution observed upwind (Figure 3), suggesting that this factor may also include distant contributions from sources situated in the Canadian side of Lake Erie, because there were no major local emission contributions upwind. Also, the resolved average number contributions at R2, R3, and Main Street (13,100; 10,500; and 9760 particles cm^{-3}, respectively) are comparable to the June 24 value measured upwind (10,200 particles cm^{-3}). As in Factor 4, Figure 8 suggests relatively steady traffic at R3 over the period considered. Factor 5, as assigned, was not resolved at R4 probably because of very low traffic counts at the time of these measurements.

Factor 6

This factor is thought to represent the size distribution of diesel agglomerates emitted from a heavy-duty diesel engine. This observation is illustrated by the high Pearson's correlation coefficients between the size distributions for this factor and "source events" related to heavy-duty diesel traffic (Table 5). The major number mode is at 70 nm

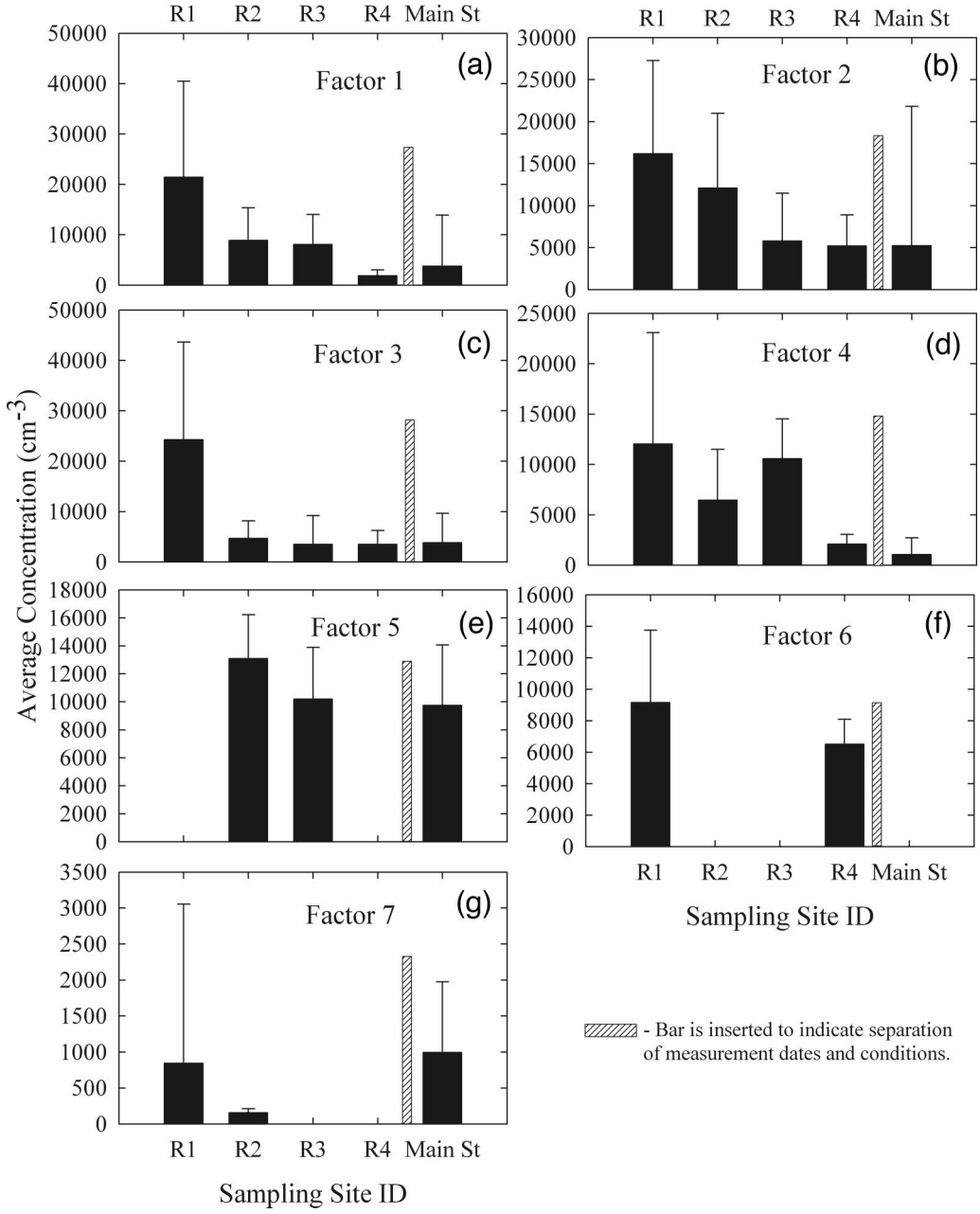

Figure 7. Average source contributions from all of the resolved factors. Error bars indicate standard deviations. (a) Factor 1; (b) factor 2; (c) factor 3; (d) factor 4; (e) factor 5; (f) factor 6; (g) factor 7.

(Figure 6), with the surface area peaking at ~100 nm. A similar size distribution has been reported by Burtscher[56] from measurements made on an engine test bench equipped with a partial flow dilution system. Morawska et al.[57] have reported average CMDs of 63, 67, and 68 nm from various types of diesel buses operating at idle, intermediate, and rated (i.e., maximum) power, respectively. The existence of a size peak at between 15 and 20 nm, observed at R1 (the source site), but not R4 (the distant site), is dependent on proximity to the combustion sources, as well as on the amount of sulfur in the fuel.[58] This peak does not show up in the surface area or volume distribution. The major number mode was higher at R1 than at R4, suggesting a strong influence of bridge emissions on this factor. R1 contributions were also relatively higher (Figure 7).

Factor 7

This factor consists mainly of accumulation and nuclei mode particles (Figure 6), and is thought to represent a mixture of locally formed and transported secondary material. The nuclei mode particles observed in this factor are believed to have resulted from atmospheric processing of local emissions. Secondary material was only resolved at R1, R2, and Main Street probably because of the high amount of tailpipe diesel emissions at these sites of which

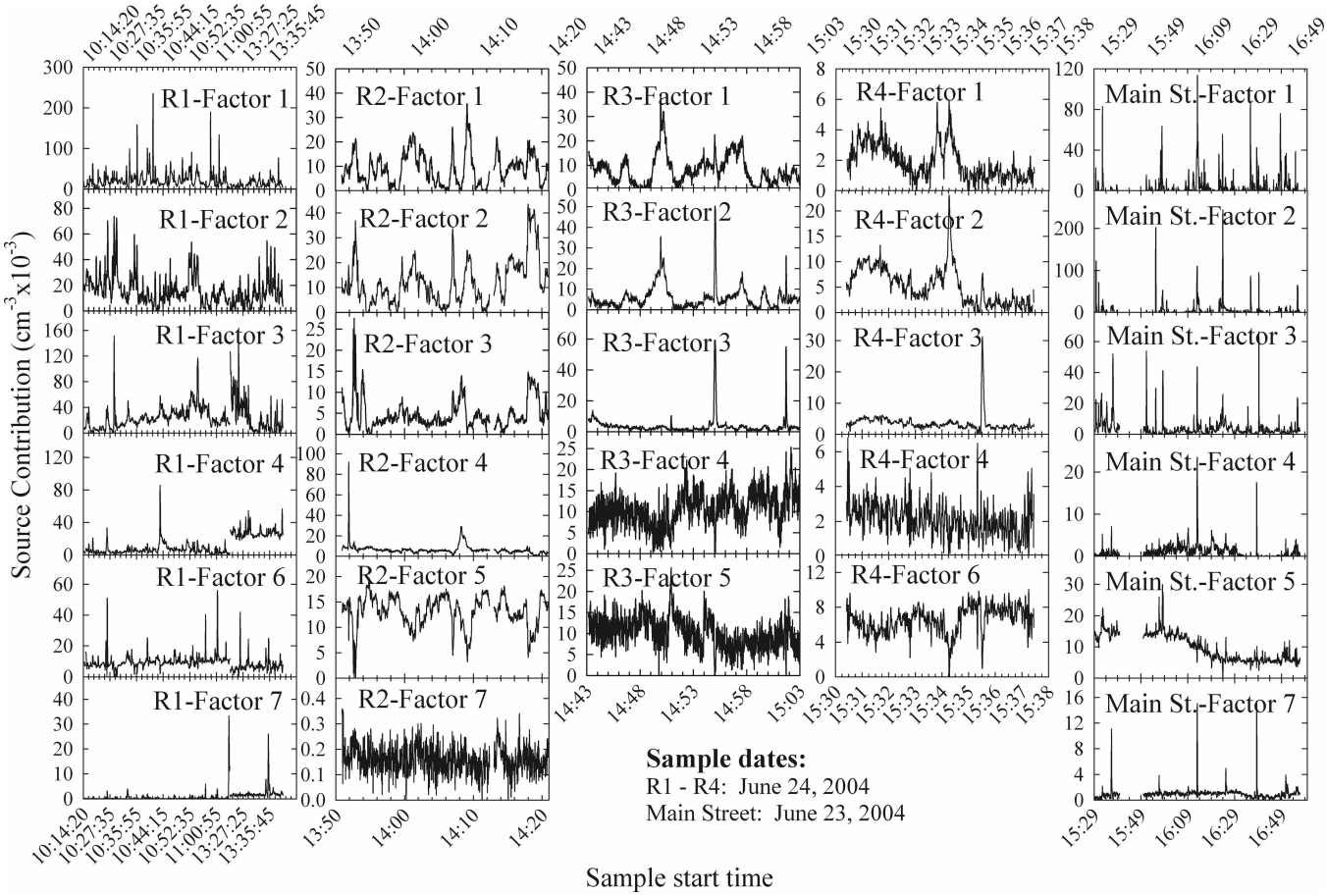

Figure 8. Source contribution time series for all the resolved factors.

the gaseous constituents may have been involved in secondary aerosol formation through nucleation and other processes at these locations. This factor was generally negatively correlated with the observed source events (Table 5) and contributed the lowest average number concentrations (Table 6 and Figure 7). Secondary diesel particles are formed during cooling in the exhaust and sampling lines.[56] Because the measurements at the five locations were made at different times and days, it is also possible that this factor represents transported material in the accumulation mode size range. It was not possible to confirm the influence of particle transport on this factor because of the short sampling period and high time resolution considered. Furthermore, it is recognized that secondary aerosol would be expected to be advected into the sampling area and, thus, would be expected to be uniform across the region of interest. However, in an area heavily influenced by local emissions, it is understandable that the model may sometimes not resolve a unique secondary material factor, particularly if its contribution is comparatively very low.

CONCLUSIONS

The present study has shown the utility of highly time-resolved particle size measurements for studying motor vehicle emissions. The highly time-resolved data have enabled size distinction between fresh versus aged vehicle exhaust and spark-ignition versus diesel emissions. A summary of the average number contributions predicted from this study has been presented.

As expected, the resolved diesel contributions are observed to be highest closest to the Peace Bridge. The magnitude of the particle number contributions closest to the Peace Bridge (i.e., site R1) may now be lower than the reported values, because the toll plaza at the PBC has been moved to the Canadian side of the United States–Canada border. Finally, it is shown that the major number mode for fresh tailpipe diesel exhaust appears to exist below the detection limit of the EEPS spectrometer and, therefore, cannot be measured at the present instrument specifications.

ACKNOWLEDGMENTS

This work was supported by the Health Effects Institute through Agreement 04-4, the New York State Energy Research and Development Authority through contract 7919, and by U.S. Environmental Protection Agency (EPA) through Science to Achieve Results Grant RD831078. Although the research described in this article has been funded wholly or in part by EPA, it has not been subjected to the agency's required peer and policy review and, therefore, does not necessarily reflect the views of the agency, and no official endorsement should be inferred.

REFERENCES

1. Oberdörster, G.; Gelein, R.; Ferin, J.; Weiss, B. Association of Particulate Air Pollution and Acute Mortality: Involvement of Ultrafine Particles?; *Inhal. Toxicol.* **1995**, *7,* 111-124.
2. Pekkanen, J.; Timonen, K.L.; Ruuskanen, J.; Reponen, A.; Mirme, A. Effects of Ultra-Fine and Fine Particles in Urban Air on Peak Expiratory Flow among Children with Asthmatic Symptoms; *Environ. Res.* **1997**, *74,* 24-33.
3. Peters, A.; Wichmann, H.E.; Tuch, T.; Heinrich, J.; Heyder, J. Respiratory Effects Are Associated with the Number of Ultrafine Particles; *Am. J. Respir. Crit. Care Med.* **1997**, *155,* 1376-1383.
4. Wichmann, H.E.; Spix, C.; Tuch, T.; Wolke, G.; Peters, A.; Herinrich, J.; Kreyling, W.G.; Heyder, J. Daily Mortality and Fine and Ultrafine Particles in Erfurt, Germany, Part A: Role of Particle Number and Particle Mass. *Health Effects Inst.* **2000**, Research Report 98.
5. Ibald-Mulli, A.; Wichmann, H.E.; Kreyling, W.; Peters, A. Epidemiological Evidence on Health Effects of Ultrafine Particles; *J. Aerosol. Med.* **2002**, *15,* 189-201.
6. Pekkanen, J.; Peters, A.; Hoek, G.; Tiittanen, P.; Brunekreef, B.; de Hartog, J.; Heinrich, J.; Ibald-Mulli, A.; Kreyling, W.G.; Lanki, T.; Timonen, K.L.; Vanninen, E. Particulate Air Pollution and Risk of ST-Segment Depression during Repeated Submaximal Exercise Tests among Subjects with Coronary Heart Disease: the Exposure and Risk Assessment for Fine and Ultrafine Particles in Ambient Air (ULTRA) Study; *Circulation* **2002**, *106,* 933-938.
7. Oberdörster, G.; Oberdörster, E.; Oberdörster, J. Nanotoxicology: an Emerging Discipline Evolving from Studies of Ultrafine Particles; *Environ. Health. Perspect.* **2005**, *113,* 823-839.
8. Nygaard, U.C.; Samuelsen, M.; Aase, A.; Løvik, M. The Capacity of Particles to Increase Allergic Sensitization Is Predicted by Particle Number and Surface Area, Not by Particle Mass; *Toxicol. Sci.* **2004**, *82,* 515-524.
9. Laden, F.; Neas, L.M.; Dockery, D.W.; Schwartz, J. Association of Fine Particulate Matter from Different Sources with Daily Mortality in Six US Cities; *Environ. Health Perspect.* **2000**, *108,* 941-947.
10. Mar, T.F.; Norris, G.A.; Koenig, J.Q.; Larson, T.V. Association between Air Pollution and Mortality in Phoenix, 1995–1997; *Environ. Health Perspect.* **2000**, *108,* 347-353.
11. Lanki, T.; de Hartog, J.J.; Heinrich, J.; Hoek, G.; Janssen, N.A.H.; Peters, A.; Stölzel, M.; Timonen, K.L.; Vallius, M.; Vanninen, E.; Pekkanen, J. Can We Identify Sources of Fine Particles Responsible for Exercise-Induced Ischemia on Days with Elevated Air Pollution? The ULTRA Study; *Environ. Health Perspect.* **2006**, *114,* 655-660.
12. McDonald, J.D.; Eide, I.; Seagrave, J.C.; Zielinska, B.; Whitney, K.; Lawson, D.R.; Mauderly, J.L. Relationship between Composition and Toxicity of Motor Vehicle Emission Samples; *Environ. Health Perspect.* **2004**, *112,* 1527-1538.
13. Sioutas, C.; Delfino, R.J.; Singh, M. Exposure Assessment for Atmospheric Ultrafine Particles (UFPs) and Implications in Epidemiologic Research; *Environ. Health Perspect.* **2005**, *113,* 947-955.
14. Kim, S.; Shen, S.; Sioutas, C.; Zhu, Y.F.; Hinds, W.C. Size Distribution and Diurnal and Seasonal Trends of Ultrafine Particles in Source and Receptor Sites of the Los Angeles Basin; *J. Air & Waste Manage. Assoc.* **2002**, *52,* 297-307.
15. Zhu, Y.; Hinds, W.C.; Kim, S.; Sioutas, C. Concentration and Size Distribution of Ultrafine Particles near a Major Highway; *J. Air & Waste Manage. Assoc.* **2002**, *52,* 1032-1042.
16. Zhu, Y.; Hinds, W.C.; Kim, S.; Shen, S.; Sioutas, C. Study of Ultrafine Particles near a Major Highway with Heavy-Duty Diesel Traffic; *Atmos. Environ.* **2002**, *36,* 4323-4335.
17. Zhu, Y.; Hinds, W.C.; Kim, S.; Shen, S.; Sioutas, C. Seasonal Trends of Concentration and Size Distribution of Ultrafine Particles near Major Highways in Los Angeles. *Aerosol Sci. Technol.* **2004,** *38*(suppl. 1), 5-13.
18. Zhang, K.M.; Wexler, A.S. Evolution of Particle Number Distribution near Roadways. Part I: Analysis of Aerosol Dynamics and Its Implications for Engine Emission Measurement; *Atmos. Environ.* **2004**, *38,* 6643-6653.
19. Kittelson, D.B.; Watts, W.F.; Johnson, J.P.; Remerowki, M.L.; Ische, E.E.; Oberdörster, G.; Gelein, R.M.; Elder, A.; Hopke, P.K.; Kim, E.; Zhao, W.; Zhou, L.; Jeong, C.-H. On-Road Exposure to Highway Aerosols. 1. Aerosol and Gas Measurements. *Inhal. Toxic.* **2004**, *16*(Suppl. 1), 31-39.
20. Kittelson, D.B.; Winthrop, F.W., Jr.; Johnson, J.P. Nanoparticle Emissions on Minnesota Highways; *Atmos. Environ.* **2004**, *38*, 9-19.
21. Bukowiecki, N.; Kittelson, D.B.; Watts, W.F.; Burtscher, H.; Weingartner, E.; Baltensperger, U. Real-Time Characterization of Ultrafine and Accumulation Mode Particles in Ambient Combustion Aerosols; *J. Aerosol Sci.* **2002**, *33,* 1139-1154.
22. Molnar, P.; Janhall, S.; Hallquist, M. Roadside Measurements of Fine and Ultrafine Particles at a Major Road North of Gothenburg; *Atmos. Environ.* **2002**, *36,* 4115-4123.
23. Hoek, G.; Brunekreef, B.; Goldbohm, S.; Fischer, P.; van den Brandt, P.A. Association between Mortality and Indicators of Traffic-Related Air Pollution in the Netherlands: a Cohort Study; *Lancet* **2002**, *360,* 1203-1209.
24. Peters, A.; von Klot, S.; Heier, M.; Trentinaglia, I.; Hörmann, A.; Wichmann, H.E.; Löwel, H. Exposure to Traffic and the Onset of Myocardial Infarction; *N. Engl. J. Med.* **2004**, *351,* 1721-1730.
25. Lwebuga-Mukasa, J.S.; Wojcik, R.; Dunn-Georgiou, E.; Johnson, C. Home Environmental Factors Associated with Asthma Prevalence in Two Buffalo Inner-City Neighborhoods; *J. Health Care Poor Underserved* **2002**, *13,* 214-28.
26. Oyana, T.J.; Rogerson, P.; Lwebuga-Mukasa, J.S. Geographic Clustering of Adult Asthma Hospitalization and Residential Exposure to Pollution at a United States-Canada Border Crossing; *Am. J. Publ. Health* **2004**, *94,* 1250-1257.
27. Oberdörster, G.; Utell, M.J. Ultrafine Particles in the Urban Air: To the Respiratory Tract—and Beyond?; *Environ. Health Perspect.* **2002,** *110,* A440-A441.
28. Swift, D.L.; Montassier, N.; Hopke, P.K.; Karpen-Hayes, K.; Cheng, Y.-S.; Su, Y.F.; Yeh, H.C.; Strong, J.C. Inspiratory Deposition of Ultrafine Particles in Human Nasal Replicate Cast; *J. Aerosol Sci.* **1992**, *23,* 65-72.
29. Cheng, Y-S.; Yeh, H.-C.; Guilmette, R.A.; Simpson, S.Q.; Cheng, K.H.; Swift, D.L. Nasal Deposition of Ultrafine Particles in Human Volunteers and Its Relationship to Airway Geometry; *Aerosol Sci. Technol.* **1996**, *25,* 274-291.
30. Kim, C.S.; Jaques, P.A. Respiratory Dose of Inhaled Ultrafine Particles in Healthy Adults; *Phil. Trans. R. Soc. Lond. A* **2000**, *358,* 2693-2705.
31. Oberdörster, G.; Sharp, Z.; Atudorei, V.; Elder, A.; Gelein, R.; Kreyling, W.; Cox, C. Translocation of Inhaled Ultrafine Particles to the Brain; *Inhal. Toxic.* **2004**, *16,* 437-445.
32. Kittelson, D.B. Engines and Nanoparticles: a Review; *J. Aerosol Sci.* **1998**, *29,* 575-588.
33. Kittelson, D.B.; Watts, W.F.; Johnson, J.P. On-Road and Laboratory Evaluation of Combustion Aerosols—Part 1: Summary of Diesel Engine Results; *J. Aerosol Sci.* **2006**, *37,* 913-930.
34. Kittelson, D.B.; Watts, W.F.; Johnson, J.P.; Schauer, J.J.; Lawson, D.R. On-Road and Laboratory Evaluation of Combustion Aerosols—Part 2: Summary of Spark Ignition Engine Results; *J. Aerosol Sci.* **2006**, *37,* 931-949.
35. Seinfeld, J.H.; Pandis, S.N. *Atmospheric Chemistry and Physics: from Air Pollution to Climate Change*; John Wiley and Sons: New York, NY, 1998; pp 51, 429-433.
36. Yao, X.; Lau, N.T.; Fang, M.; Chan, C.K. Real-Time Observation of the Transformation of Ultrafine Atmospheric Particle Modes; *Aerosol Sci. Technol.* **2005**, *39,* 831-841.
37. Paatero, P. Least Squares Formulation of Robust Non-Negative Factor Analysis; *Chemom. Intell. Lab. Syst.* **1997**, *37,* 23-35.
38. Sakurai, H.; Tobias, H.J.; Park, K.; Zarling, D.; Docherty, K.S.; Kittelson, D.B.; McMurry, P.H.; Ziemann, P.J. On-Line Measurements of Diesel Nanoparticle Composition and Volatility; *Atmos. Environ.* **2003**, *37,* 1199-1210.
39. Johnson, J.P.; Kittelson, D.B.; Watts, W.F. Source Apportionment of Diesel and Spark Ignition Exhaust Aerosol Using On-Road Data from the Minneapolis Metropolitan Area; *Atmos. Environ.* **2005**, *39,* 2111-2121.
40. Lee, D.; Miller, A.; Kittelson, D.; Zachariah, M.R. Characterization of Metal-Bearing Diesel Nanoparticles Using Single-Particle Mass Spectrometry; *J. Aerosol Sci.* **2006**, *37,* 88-110.
41. Yao, X.; Lau, N.T.; Fang, M.; Chan, C.K. On the Time-Averaging of Ultrafine Particle Number Size Spectra in Vehicular Plumes; *Atmos. Chem. Phys. Discuss.* **2006**, *6,* 6825-6839.
42. Su, D.S.; Müller, J.-O.; Jentoft, R.E.; Rothe, D.; Jacob, E.; Schlögl, R. Fullerene-Like Soot from EuroIV Diesel Engine: Consequences for Catalytic Automotive Pollution Control; *Topics Catalysis* **2004,** *30/31*, 241-245.
43. Johnson, T.; Caldow, R.; Pocher, A.; Mirme, A.; Kittelson, D.B. A New Electrical Mobility Particle Sizer Spectrometer for Engine Exhaust Particle Measurements. *SAE-SP-1871: Test Instrument* **2004,** 2004-01-1341.
44. Kittelson, D.B.; Watts, W.F.; Johnson, J.P.; Rowntree, C.; Payne, M.; Goodier, S.; Warrens, C.; Preston, H.; Zink, U.; Ortiz, M.; Goersmann, C.; Twigg, M.V.; Walker, A.P.; Caldow, R. On-Road Evaluation of Two Diesel Exhaust after-Treatment Devices. *J. Aerosol Sci.* **2006**, *37*, 1140-1151.
45. Jeong, C.-H.; Hopke, P.K.; Chalupa, D.; Utell, M. Characteristics of Nucleation and Growth Events of Ultrafine Particles in Rochester, NY; *Environ. Sci. Technol.* **2004**, *38,* 1933-1940.
46. Jeong, C.-H.; Evans, G.J.; Hopke, P.K.; Chalupa, D.; Utell, M. Influence of Atmospheric Dispersion and New Particle Formation Events on Ambient Particle Number Concentration in Rochester, USA and Toronto, Canada; *J. Air & Waste Manage. Assoc.* **2006**, *56,* 431-443.
47. Ogulei, D.; Hopke, P.K.; Chalupa, D.C.; Utell, M. Modeling Source Contributions to Submicron Particle Number Concentrations Measured in Rochester, NY; *Aerosol Sci. Technol.*, in press.
48. Woo, K.S.; Chen, D.R.; Pui, D.Y.H., McMurry, P.H. Measurement of Atlanta Aerosol Size Distributions: Observations of Ultrafine Particle Events; *Aerosol Sci. Technol.* **2001**, *34,* 75-87.

49. Stanier, C.O.; Khlystov, A.Y.; Pandis, S.N. Ambient Aerosol Size Distributions and Number Concentrations Measured during the Pittsburgh Air Quality Study (PAQS); *Atmos. Environ.* **2004**, *38,* 3275-3284.
50. Ondov, J.M.; Buckley, T.J.; Hopke, P.K.; Ogulei, D.; Parlange, M.B.; Rogge, W.F.; Squibb, K.S.; Johnston, M.V.; Wexler, A.S. Baltimore Supersite: Highly-Time and Size Resolved Concentrations of Urban $PM_{2.5}$ and Its Constituents for Resolution of Sources and Immune Responses. *Atmos. Environ.* **2006**, *40*(Suppl. 2), 224-237.
51. Ogulei, D.; Hopke, P.K.; Wallace, L.A. Analysis of Indoor Particle Size Distributions in an Occupied Townhouse Using Positive Matrix Factorization; *Indoor Air* **2006**, *16,* 204-215.
52. Paatero, P.; Hopke, P.K.; Begum, B.A.; Biswas, S.K. A Graphical Diagnostic Method for Assessing the Rotation in Factor Analytical Models of Atmospheric Pollution; *Atmos. Environ.* **2005**, *39,* 193-201.
53. Jamriska, M.; Morawska, L.; Thomas, S.; He, C. Diesel Bus Emissions Measured in a Tunnel Study; *Environ. Sci. Technol.* **2004**, *38,* 6701-6709.
54. Zhang, K.M.; Wexler, A.S.; Zhu, Y.F.; Hinds, W.C.; Sioutas, C. Evolution of Particle Number Distribution near Roadways. Part II: The 'Road-to-Ambient' Process; *Atmos. Environ.* **2004**, *38,* 6655-6665.
55. Ristovski, Z.D.; Morawska, L.; Bofinger, N.D.; Hitchins, J. Submicrometer and Supermicrometer Particulate Emission from Spark Ignition Vehicles; *Environ. Sci. Technol.* **1998**, *32,* 3845-3852.
56. Burtscher, H. Physical Characterization of Particulate Emissions from Diesel Engines: a Review; *J. Aerosol Sci.* **2005**, *36,* 896-932.
57. Morawska, L.; Bofinger, N.D.; Kocis, L.; Nwankwoala, A. Submicrometer and Supermicrometer Particles from Diesel Vehicle Emissions; *Environ. Sci. Technol.* **1998**, *32,* 2033-2044.
58. Ristovski, Z.D.; Jayaratne, E.R.; Lim, M.; Ayoko, G.A.; Morawska, L. Influence of Diesel Fuel Sulfur on Nanoparticle Emissions from City Buses; *Environ. Sci. Technol.* **2006**, *40,* 1314-1320.

About the Authors

David Ogulei is a doctoral candidate and Philip K. Hopke is the Bayard D. Clarkson Distinguished Professor and Director of the Center for Air Resources Engineering and Science, both in the Department of Chemical and Biomolecular Engineering at Clarkson University. Peter A. Jaques is with the Department of Biology and Andrea R. Ferro is with the Department of Civil and Environmental Engineering, both at Clarkson University. Address correspondence to Philip K. Hopke, Center for Air Resources Engineering and Science, Clarkson University, P.O. Box 5708, Potsdam, NY 13699-5708; phone: +1-315-268-3861; fax: +1-315-268-4410; e-mail: hopkepk@clarkson.edu.